Thermally Driven Natural Circulation Water Pump

K Hobbs, R T Dobson

Department of Mechanical and Mechatronic Engineering, University of Stellenbosch,

Private Bag X1, MATIELAND 7602, South Africa

Tel 27 21 808 4268, Fax 0866 155 206, e-mail rtd@sun.ac.za

Abstract

The water utilized by passive air-conditioning systems in buildings is typically required at higher elevations. The thermally driven natural circulation water pump (TDNCWP) is a passively driven pumping system for delivering water from ground level against gravity to a higher elevation. The TDNCWP is shown by theoretical and experimental work to provide water at varied elevations using non-mechanical, passive means. Experiments were conducted on two experimental TDNCWP set-ups of different cross-sectional areas to evaluate the pump design and the theoretical model. A temperature difference of 9 to 12.5 °C between the heating and cooling sections induced an average velocity of 0.4 to 0.6 m/s for a duct cross section of 100 mm^2. For a larger cross section of 400 mm^2, a temperature difference of 2 to 5 °C induced an average velocity of 0.25 to 0.3 m/s. An asymmetrical velocity profile was observed which varied at different points in the loop. A water delivery rate of 1.2 to 7.5 L/day was experimentally determined. This compares well to the passive air-conditioning water requirements of a small building. The theoretical model over-predicted the delivery rate at increased duct cross-sectional areas but fared well when compared to the smaller experimental model results. Further refinement of the numerical model and the TDNCWP design is required, and recommendations were made regarding this. It is clear however that the TDNCWP provides an alternative to a conventional water pump for low-volume water pumping requirements.

Keywords: Green building, Air-conditioning, Pump, HVAC, PDEC

1 INTRODUCTION

Green building design is a manner of designing structures and using operational practices which are energy efficient, resource efficient and environmentally responsible[1]. The design philosophy is to utilize renewable, energy conscious and sustainable design methods for buildings with a focus on reducing the energy consumption and reducing climate changing effects. In South Africa, the building sector accounts for 23 % of the total green house gas emissions[2]. A conventional, energy intensive practice in the built environment is that of Heating, Ventilation and Air-Conditioning (HVAC). HVAC systems are ergonomic systems utilized with intent to improve the comfort and productivity of the occupants. HVAC systems condition the environment in a building by changing the temperature, humidity and quality of the internal air as well as the rate of air movement within the building. In South Africa, the electricity used by HVAC systems is primarily generated from fossil-fuels, which produce climate changing emissions. The actual electricity usage of HVAC systems in South Africa[3] is around 15% of peak power consumption, or 5 400 MW. However, the specific energy usage of a typical HVAC system depends largely on the building utilization, where it can account for up to 54% of the total building usage in an office building housing 1 600 people over 4 265 m^2 floor area[4]. Furthermore, this energy usage can account for approximately 50% of the total life cycle cost[5] of the HVAC system, depending on the installation and usage. Energy management control systems can be employed to mitigate this high energy consumption and cost. However, a trend analysis[6] on a typical HVAC system revealed that even with a control system in place high energy consumption can still occur through unforeseen losses. An alternative to conventional HVAC systems in buildings is the passive downdraft evaporative cooling (PDEC) system. The Torrent research centre in Ahmedebad, India is one example of an installed PDEC system. The PDEC system utilizes natural phenomena such as density, gravitation and evaporative cooling to condition the air ventilating a building. In this system, towers are used to draw in outside air through chamber where evaporative cooling occurs by use of wetted pads or water misters. This cooled air ventilates the building, where it is heated by the internal building load before being exhausted by use of outlet towers. The inlet air can be cooled to within 70 to 80% of the inlet wet bulb temperature[7] when sufficient water is provided for evaporation. The water used

in the PDEC system is required at roof level, such that the water-cooled air can sink into the building. The volumetric water requirements for PDEC systems in order to facilitate the evaporative cooling varies greatly depending on the climate, cooled air volume, internal loading, desired indoor temperature and method of water evaporation. For a single room space, with the same inlet conditions, design conditions and typical room loading, the water requirements[8] range from 85 L/day for a 396 m^3 classroom to 143 L/day for a 7 904 m^3 auditorium. The water required per volume of cooled space is therefore indicated to decrease with increasing air volume or larger building size. Typical values[7,9,10] for a variety of building size and design loading are shown in Table 1

Table 1: Indicative PDEC system water requirements for various buildings[7,9,10]

Building description	Design cooling load	Actual water requirements
Large, multi-story	20.9 kWh/m^2	10L/day/person
	8 kWh/m^2	1L/day/person
	631.1 kWh/annum	6029L/annum
Small, single- storey	1.85 kWh/m^2	38L/day
	2.42 kWh/m^2	50L/day

As the water is required at roof level, an electric pump is often utilized to provide the water. In a study by Kang[11] it was found that 150 to 250 W of pumping power is required for PDEC towers at 5 to 8 m above ground. In addition to energy costs, pumps also required frequent maintenance and a reliable supply of electrical energy. With the exception of this pump, a typical PDEC system requires no electrical input and is a completely sustainable process for conditioning the air entering a building. The thermally driven natural circulation water pump (TDNCWP) system is proposed as an alternative to the conventional water pump, and is an electricity free manner of moving the required water for the PDEC system. This research further explores the surmised TDNCWP system, with the objectives of this research being to:

- Design, construct and test experimental models of the Thermally Driven Natural Circulation Water Pump (TDNCWP)
- By use of experimental data, determine the feasibility of using a simple one-dimensional theoretical model to simulate the TDNCWP system
- Evaluate the daily water delivery capabilities of the TNDCWP

2 MECHANISM

The TDNCWP concept utilizes natural air circulation and renewable energy resources to supply the required water for the PDEC system. As illustrated in Figure 1, the TDNCWP configuration surmised is physically structured as a closed loop air duct system consisting of four sections with square cross sectional profile. A vertical tower heating section is heated by use of solar radiation on one of the outside walls, which transfers through the wall into the loop. The opposite vertical cooling section is subjected to a relatively cooler environment, which is surmised to be on all four walls. The temperature difference between the average heating and cooling section temperatures $\overline{T}_{heat}$ and $\overline{T}_{cool}$ creates buoyancy driven natural circulation flow G in the clockwise direction. At ground level water in a horizontal water tray within the duct is evaporated to the air aided by the use of a passive solar water heating system, such as a solar geyser. This humid air flows through the loop roof level, where water vapour is condensed from this air using a cold plate. The cold plate can be maintained at a cooler temperature by use of ambient water from a shaded tank in a natural circulation water loop, or use of a night sky radiation cooling system. The water which condenses on the cold plate is then collected, pipes out of the loop and routed to the PDEC system. Water is therefore moved from ground to roof level using natural occurring phenomena.

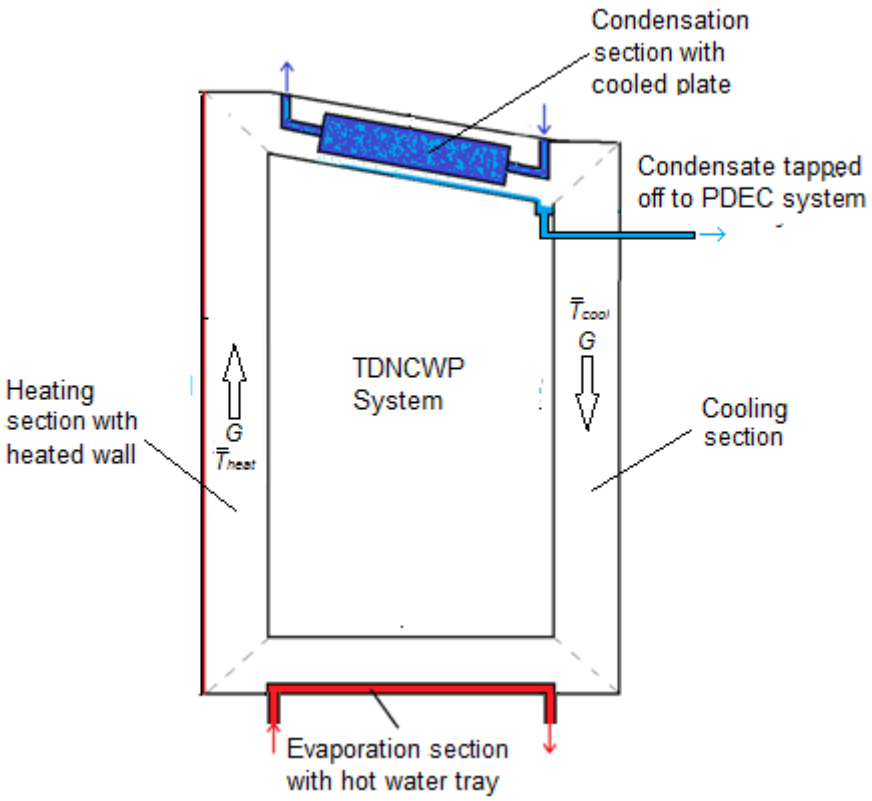

Figure 1 The thermally driven natural circulation water pump

In understanding the TDNCWP mechanism, the fundamental momentum, energy and mass transfer principles need to be understood. The local effects in the loop are dependent on the bulk flow rate, which in turn is effected by the local friction as well as the friction and heat and mass transfer everywhere else in the loop. There is therefore a strong coupling of the local conditions with those everywhere else in the system. This occurs through the interaction of the local momentum, energy and mass transfer at each section with the rest of the loop occurs through the flow of air. The pumping ability of the overall TDNCWP system is therefore dependent on all these elements. When considering friction, the velocity profile affects the overall losses. For the vertical sections, an axisymmetrical velocity profile with 4 local maxima was found for developed flow and boundary conditions similar to that of the TDNCWP cooling section[12]. For the TDNCWP heating section, a large flow bias was observed towards the heated wall[12] with reversed flow possible on the opposite surface due to the buoyancy effects. These results may be affected by the elbows linking each section, which could be mitigated by the use of guide vanes[13]. For the horizontal sections, the friction magnitude is seen to oscillate with flow direction before approaching asymptotic values[14]. The bulk loop flow is due to average temperature difference across the loop where this is directly dependent on heat transfer at each section. The heat transfer changes the temperature profile of the flow, which is directly related to the Nusselt number. For developed vertical duct flow with boundary conditions similar to that in the TDNCWP this profile is observed to be axisymmetrical for the cooling section and bias towards the heated wall in the heating section[12]. For the horizontal sections, the bulk flow interacts with local, orthogonal buoyancy flows. This affects the Nusselt number, causing an oscillation before approaching asymptotic values[15]. Both the heat transfer and velocity effects in the loop effect the mass transfer at the cold plate and the water surface, which is directly related to the pumping capacity of the TDNCWP. However, direct relations for the mass transfer depend on the flow regime and flow length[16], the water temperature and air humidity[17] as well as the surface conditions and flow velocity with numerous relations proposed for evaporation off a water surface[18,19,20,21]. It was also found that it was possible to use the same relations utilized for heat transfer in calculating the mass transfer rate[22,23].

3 THEORETICAL MODEL

A one-dimensional theoretical model is developed based on the conservation equations as well as friction, heat and mass transfer equations[23] for one-dimensional flow. Forced convection heat and mass transfer is assumed on the internal surfaces, and natural convection heat transfer on the external walls. Friction is calculated utilizing those provided for internal flow conditions, with all flow assumed as quasi-steady and parallel to the duct walls at some average flow rate everywhere in the loop. Airflow properties are found using 5th order curve fits found in literature[23] and the humid air viscosity, conductivity and specific heat are found by further relations[24]. A numerical simulation program is then utilized to solve the theoretical model equations across small control volumes. These control volumes are formed by discretizing the entire flow domain around the TDNCWP loop into N computational domains as seen in Figure 2.

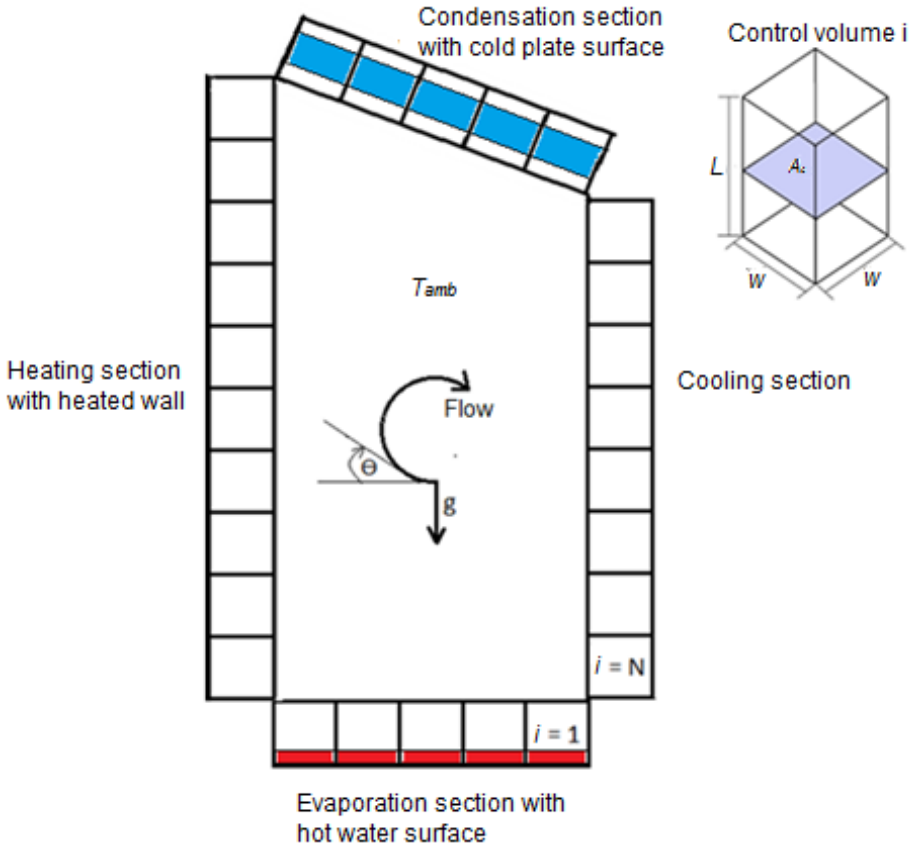

Figure 2 Discretization schematic of the flow domain

A time dependent model with an explicit discretization method is utilized in the numerical program to solve these coupled equations. Numerical accuracy is improved by performing grid and time step independence tests. Numerical convergence can be seen when a steady temperature, velocity and condensate rate result and is confirmed by calculating an energy balance of the system, where a zero balance is indicative of convergence.

Conservation of momentum: By applying the conservation of momentum to the TDNCWP loop, the flow rate at each time step can be determined. The assumptions regarding the fluid flow later stated in section 4.1 are incorporated in order to develop the theoretical model equations utilized in the numerical model. The conservation of linear momentum as defined[23] in one dimension for a control volume is:

$$\frac{d}{dt}(mv)_{sys} = \sum F_{R,sys} \tag{1}$$

The conservation of momentum diagram applied to a typical control volume in the TDNCWP loop is shown in Figure 3 with θ as defined in Figure 2.

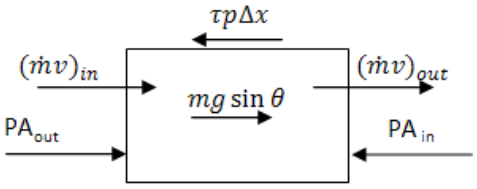

Figure 3 Conservation of momentum applied to each control volume

The forces which act on a control volume of fluid can be divided into body, surface and other external forces. Using the forces shown in Figure 3, equation (1) can therefore be restated for a typical control volume as:

$$\frac{d(mv)}{dt} = (\dot{m}v)_{in} - (\dot{m}v)_{out} + (P_{out} - P_{in})A_C + mg\sin\theta - \tau pL \tag{2}$$

The shear stress due to friction can be described by:

$$\tau_i = \frac{C_f \rho v^2}{2} \tag{3}$$

Noting that $m = \rho A_C L$ and $\dot{m} = \rho v A_C = \rho G$, substitution of equation (3) into equation (2) and division through by A_C yields for each control volume i:

$$\frac{d}{dt}\left(\frac{mG}{A_C^2}\right)_i = \left[\left(\frac{\rho G^2}{A_C^2}\right)_{in} - \left(\frac{\rho G^2}{A_C^2}\right)_{out} + (P_{out} - P_{in}) - \left(\frac{C_f \rho G^2}{2A_C^2}\right)\left(\frac{pL}{A_C}\right)\right]_i \tag{4}$$

Integration around the closed loop is possible as the volumetric flow rate is assumed to be the same at every control volume for each time step. This further cancels out the pressure term as the summation of around a closed loop is zero. Discretization of the resulting equation every control volume i in the loop then yields:

$$\sum_{i=1}^{N} \frac{\Delta}{\Delta t}\left[\frac{mG}{A_C^2}\right]_i = [M + B - F]_i \tag{5}$$

The mass M, gravitational force B and friction F terms are defined by:

$$M = \sum_{i=1}^{N}\left[\left(\frac{\rho G^2}{A_C^2}\right)_{in} - \left(\frac{\rho G^2}{A_C^2}\right)_{out}\right]_i \tag{6}$$

$$B = \sum_{i=1}^{N}(\rho \Delta x g \sin\theta)_i \tag{7}$$

$$F = \sum_{i=1}^{N}\left[\left(\frac{C_f \rho G^2}{2A_C^2}\right)\left(\frac{p(L+L_{minor})}{A_C}\right)\right]_i \tag{8}$$

An additional frictional loss L_{minor} is introduced to account for minor losses due to the corners and obstructions. Momentum change terms M1 and M2 are then defined as:

$$M1 = \sum_{i=1}^{N}\left(\frac{m_i^{t+\Delta t}}{A_{C,i}^2}\right) \tag{9}$$

$$M2 = \sum_{i=1}^{N}\left(\frac{m_i^{t}}{A_{C,i}^2}\right) \tag{10}$$

The momentum change term of the LHS of equation (5) can then be modified to form:

$$\sum_{i=1}^{N} \frac{\Delta}{\Delta t}\left[\frac{mG}{A_C}\right] = \frac{G^{t+\Delta t}M1 - G^{t}M2}{\Delta t} \tag{11}$$

Equations (5) and (11) can then be combined, and the resulting equation for the flow rate in the loop is:

$$G^{t+\Delta t} = \frac{G^{t}M2}{M1} + \Delta t \frac{(M+B-F)^{t}}{M1} \tag{12}$$

One observes that equation (12) then relates the volumetric flow rate at each control volume in the loop to the friction, buoyancy as well as the mass and density changes at every control volume in the loop. The newly calculated flow rate is then used to find the flow velocity and mass flow rate at the new time step.

Conservation of energy: Energy flow into and out of the TDNCWP system is in the form of convective heat transfer and mass-energy transfer. Convection heat transfer occurs on the inside and outside of the TDNCWP loop, and mass-energy transfer is possible where there is evaporation and condensation. The conservation of energy as applied to every control volume in the TDNCWP loop is shown in Figure 4.

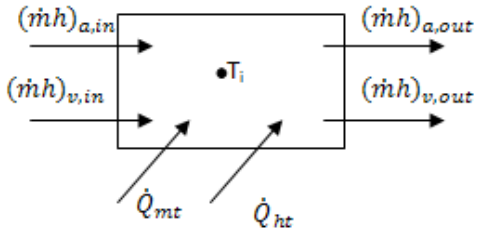

Figure 4 Conservation of energy applied to each control volume

The conservation of energy equation can be defined[23] for a control volume as:

$$\frac{\partial E}{\partial t} = \dot{Q}_{NET} + \dot{W}_{NET} + \left(\dot{m}(u + \frac{v^2}{2} + gz)\right)_{NET} \tag{13}$$

The heat transfer and work terms in Figure 4 can be described by:

$$\dot{Q}_{NET} = \dot{Q}_{ht,in} - \dot{Q}_{ht,out} + \dot{Q}_{mt,in} - \dot{Q}_{mt,out} \tag{14}$$

$$\dot{W}_{NET} = \dot{W}_{in} - \dot{W}_{out} + \dot{W}_{fluid,in} - \dot{W}_{fluid,out} - \dot{W}_{walls} \tag{15}$$

The work done on the internal walls due to pressure changes is assumed to be negligible. Flow energy can be defined as the work done by pressure to displace a body of fluid, and is described by the following equation:

$$\dot{W}_{fluid,NET} = \dot{W}_{fluid,in} - \dot{W}_{fluid,out} = \dot{m}PV_{in} - \dot{m}PV_{out} \tag{16}$$

Further to this, enthalpy of a flowing fluid can be described as:

$$h = u + PV \tag{17}$$

The change in velocity *v* can be neglected as the flow rate is assumed constant everywhere in the loop and the area is constant in each section. The change in height z over a control volume is also neglected due to the low density of the humid air. Using Figure 4, equation (13) can then be combined with equations (14) to (17) to form the energy change formula for each control volume in the loop:

$$\left(\frac{\partial E}{\partial t}\right)_i = \left[\dot{Q}_{ht,NET} - \dot{Q}_{mt,NET} + \dot{W}_{in} - \dot{W}_{out} + (\dot{m}h)_{in} - (\dot{m}h)_{out}\right]_i \tag{18}$$

The mass-enthalpy can be divided into that for the air and vapour portions of the flowing humid air. The energy change of the control volume can be described by:

$$\frac{\partial E}{\partial t} = \frac{\partial}{\partial t}(mc_PT) = mc_P\frac{dT}{dt} + c_PT\frac{dm}{dt} + mT\frac{dc_P}{dt} \tag{19}$$

Substitution of equation (4.20) and equation into equation (4.19), and discretization for control volume i using the explicit numerical method yields:

$$T_i^{t+\Delta t} = T_i^t + \frac{\Delta t}{(mc_P)_i^t} \left[T1 + T2 - T_i^t \left(c_P \frac{dm}{dt} + m \frac{dc_P}{dt}\right)\right]_i^t \tag{20}$$

The temperature changed terms $T1$ and $T2$ can be defined as:

$$T1_i^t = \left(\dot{Q}_{ht,NET} - \dot{Q}_{mt,NET}\right)_i^t \tag{21}$$

$$T2_i^t = \left[(\dot{m}h)_{a,in} - (\dot{m}h)_{a,out} + (\dot{m}h)_{va,in} - (\dot{m}h)_{va,out}\right]_i^t \tag{22}$$

The change in specific heat term in can be discretized as:

$$\left(\frac{dc_P}{dt}\right)_i^t = \frac{{c_P}_i^{t+\Delta t} - {c_P}_i^t}{\Delta t} \tag{23}$$

Noting that the specific heat at constant volume is calculated at a specific temperature, the term ${c_P}_i^{t+\Delta t}$ cannot be explicitly evaluated. However, it is assumed that the term can be linearly approximated with reasonable accuracy based on the specific heat at the previous two time steps and temperatures. The mass-energy transfer $\dot{Q}_{mt,NET}$ in equation (21) is the energy transfer due to phase changes that occur due to evaporation and condensation at the hot water tray and cold plate respectively. The mass transfer rate, calculated in section 4.4, can be used to determine the overall mass-energy transfer by[23]:

$$\dot{Q}_{mt,i} = \sum_{s=1}^{S} (\dot{m}_{mt} h_g)_{(i,s)} \tag{24}$$

The enthalpy of the water which changes phase is found by property relations, where it is evaluated at the temperature of the mass transfer surface for evaporation, and the internal humid air temperature for condensation. The heat transfer $\dot{Q}_{ht,NET}$ in equation (24) is that between the internal air and the walls. In order to determine this, a generalized thermal network is constructed for every control volume, as observed in Figure 5. It can be observed that for every control volume there is then a system of four heat transfer equations.

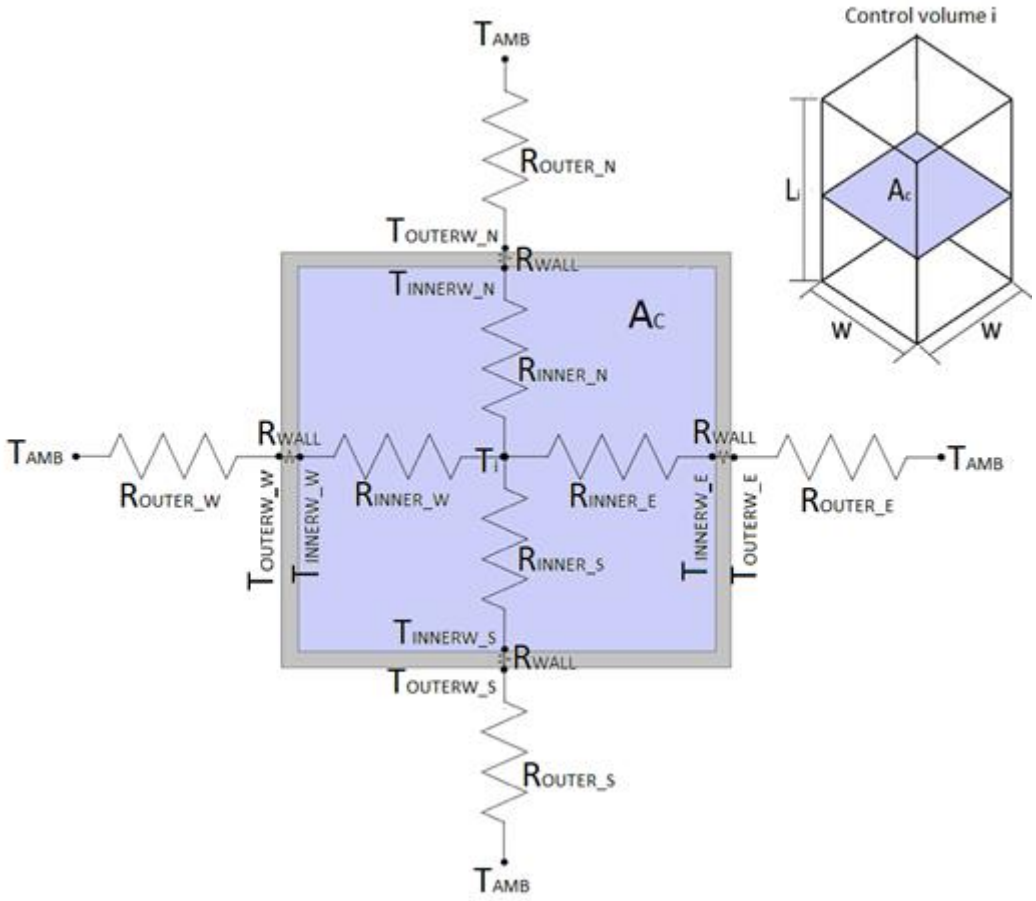

Figure 5 Generalized thermal resistance network for control volume *i*

The thermal resistance values shown in Figure 5 associated with the internal convection, wall conduction and external convection heat transfer mechanisms can be computed by the following,

$$R_{cond} = R_{wall,i} = \frac{t_p}{k_p A_{wall,i}} \tag{25}$$

$$R_{conv,outer} = R_{outer,(i,s)} = \frac{1}{h_{ht-outer,(i,s)} A_{wall,i}} \tag{26}$$

$$R_{conv,inner} = R_{inner,(i,s)} = \frac{1}{h_{ht-inner,(i,s)} A_{wall,i}} \tag{27}$$

where the heat transfer area for each wall is $A_{wall,i} = L_i\, w$. The heat transfer at each wall can therefore be found between any two known temperatures by:

$$\dot{Q}_{ht,1-2} = \frac{T_1 - T_2}{R_{1-2}} \tag{28}$$

The terms T_1 and T_2 are the known temperatures and R_{1-2} is the sum of all resistances between the two temperatures. For the wall heat transfer, the conductivity of the TDNCWP walls are assumed to be constant for the temperature ranges expected. The conductive resistance is therefore constant for all temperatures. The convection heat transfer resistance of a surface is a function of the surface area and the coefficient of convective heat transfer. The coefficient of heat transfer calculated from the Nusselt number by[23]:

$$h_{ht,(i,s)} = \left(\frac{k_{fluid}}{D_h} Nu\right)_{i,s} \tag{29}$$

The forced internal flow Nusselt number relations are utilized for all the internal surfaces and natural flat plate Nusselt number relations are used for the external wall surfaces. Using this method, the magnitude of heat transfer across the TDNCWP walls is calculated between the ambient air temperature and the internal air temperature. The heat transfer due to the heated wall, cold plate and hot water tray is similarly found. The heat transfer with each control volume is then the summation of the heat transfer through every surface in that control volume.

Conservation of momentum: Mass transfer in the TDNCWP loop occurs at the hot water tray, cold plate and the walls of the condensation section. The conservation of mass as applied to every control volume in the TDNCWP loop is shown in Figure 6.

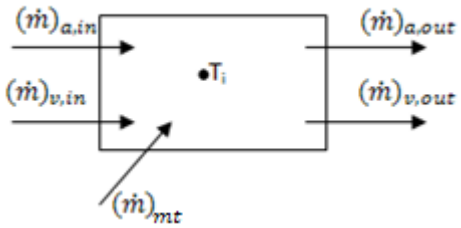

Figure 6 Conservation of mass applied to each control volume

The conservation of mass equation can be defined[23] for a fixed control volume as:

$$\frac{d}{dt}\int_{\mathrm{cv}} \rho \, dV + \int_{\mathrm{cs}} \rho v \, dA = 0 \tag{30}$$

Applying the assumption that the flow is one-dimensional through a constant volume, and using the explicit numerical method, equation (30) is discretized to become:

$$\frac{dm}{dt} = \sum \dot{m}_{in} - \sum \dot{m}_{out} \tag{31}$$

The finite difference approximation of equation (31) using an explicit numerical method results in:

$$m_i{}^{t+\Delta t} = m_i + \Delta t(\dot{m}_{i-1} - \dot{m}_i) \tag{32}$$

Equation (32) is for the total mass in control volume *i*, and it can be separated into equations for both the air and water vapour components of the bulk flow. Equations for the new vapour and air masses can then be defined by:

$$m_{v,i}{}^{t+\Delta t} = m_{v,i} + \Delta t(\dot{m}_{v,i-1} - \dot{m}_{v,i} + \dot{m}_{mt,i}) \tag{33}$$

$$m_{a,i}{}^{t+\Delta t} = m_{a,i} + \Delta t(\dot{m}_{a,i-1} - \dot{m}_{a,i}) \tag{34}$$

The mass transfer term in equation (33) is calculated for every control volume i for surface s by the following equation[23]:

$$\dot{m}_{mt,(i,s)} = h_{mt,i} A_{mt,i} \left(\rho_{v,sat@T_s} - \rho_{v@T_i}\right)_i \tag{35}$$

Equation (35) is defined positive for evaporation. The density terms are calculated by ideal gas laws,

$$\rho_{v@T_i,i} = \left(\frac{m_{v,i}}{V_i}\right)_{T_i,i} \tag{36}$$

$$\rho_{v,sat@T_s,i} = \left(\frac{P_{v,sat@T_s}}{\mathrm{R}_v T_s}\right)_i \tag{37}$$

The mass transfer coefficient for control volume i is determined by[23]:

$$h_{mt,i} = \left(\frac{Sh\, D_{v-a}}{D_h}\right)_i \quad (38)$$

4 EXPERIMENTAL WORK

Experiments are conducted on two laboratory-standard thermally driven natural circulation water pump (TDNCWP) experimental models of different sizes. The models were designed such that the internal dry bulb temperature, wet bulb temperature, velocity as well as the overall condensate production could be determined. The geometric properties of both the models are shown in Table 2. The experimental models are of different size, with model 'A' being the smaller with loop dimensions of 2.8 x 1.4 m. Model 'B' is the larger model with loop dimensions of 5.8 x 3 m. It can also be seen that model B's duct length to width ratio is less than the model A loop. Both models of square cross section, and have a similar evaporation to condensation area ratio, which is important for the overall water supply.

Table 2 Geometric properties and of the experimental models

Parameter	Model A	Model B
Max vertical height (m)	2.8	5.8
Max horizontal width (m)	1.4	3
Declined condensate section angle	12.5°	12.8°
Total duct centreline length (m)	8.2	16.2
Duct cross sectional dimensions (mm)	100x100	400x400
Centreline length to cross sectional width ratio	82	40.5
Average wall thickness (mm)	2	2.5
Total duct centreline length (m)	8.2	16.2
Water tray free surface area (m^2)	0.12	0.68
Fin area (m^2)	0.072	0.54
Evaporation to condensation areas ratio	1.67	1.26
Heating wall area (m^2)	0.28	1.76

The smaller TDNCWP experimental model A is shown in Figure 7. Model A's closed duct loop system is constructed from angle iron and acrylic plastic sheets, with cross sectional duct dimensions of 100 x 100 mm. The vertical heating wall is the outside wall of the heating section on the left in Figure 7. The vertical cooling section is the right hand channel in Figure 7, and is subjected only to ambient air. The cold plate is housed in the condensate section at the top. The cold plate is comprised of a central copper pipe with flat copper plates welded to it. It is connected to a cold water supply system by piping in order to maintain a cool temperature relative to the internal humid air. Condensate from the cold plate and duct walls is collected at the lower end of this section through a hole in the bottom wall. A hot water tray with copper pipe heat exchanger is housed in the horizontal evaporation section. The heat exchanger in the water tray is connected to a hot water supply system by piping in order to maintain the water temperature in the tray. This tray is manually filled with fresh water, with the water surface exposed to the humid air within the TDNCWP loop.

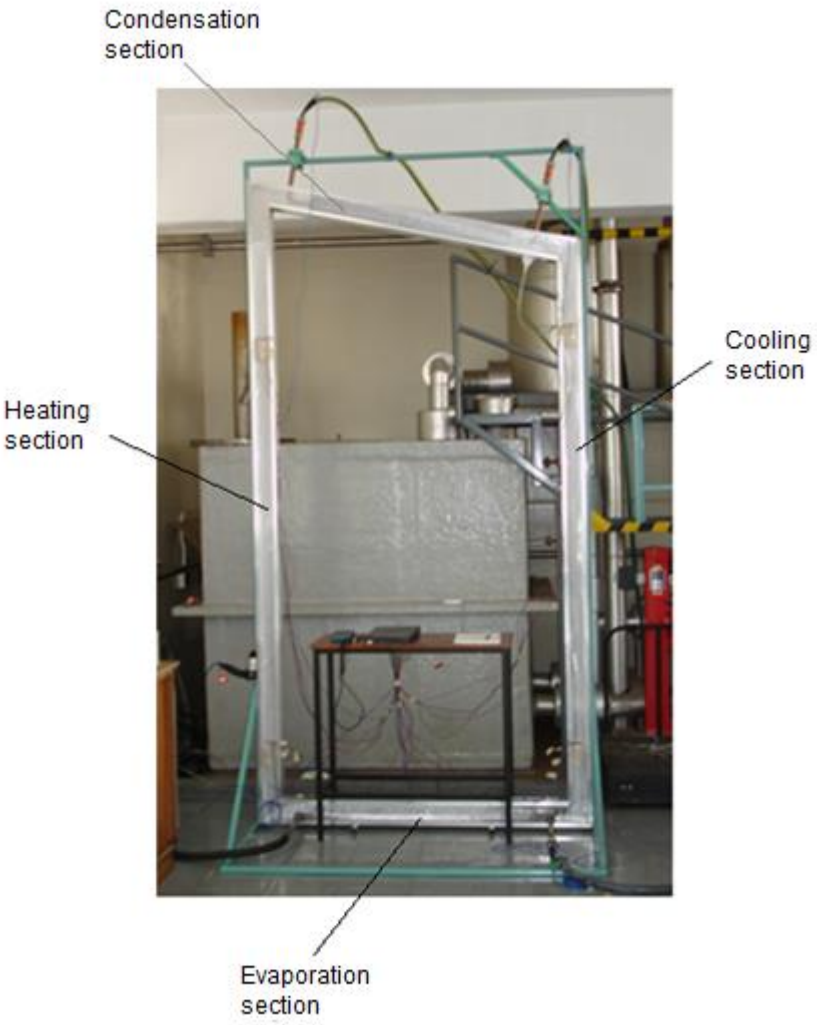

Figure 7 Picture of model A

A schematic indicating the measurement points is shown in Figure 8. Air velocities are found at the mid-height cross section of the left and right sections on a planar grid at five points. Twenty type-t thermocouples were placed as indicated in Figure 8 such that the average dry and wet bulb temperatures in each section can be determined. The cold and hot water supply and return temperatures are monitored, as well as the mass flow rate in these pipes. The thermocouples are removable so that they can be used to take other temperature readings such as the ambient temperature in the laboratory. The wall heating system is additionally observed. The small experimental model provided a good model for evaluating the TDNCWP mechanism. However, in order to compare the possible effects of scale and irregularities that may occur in the flow, a larger model is required.

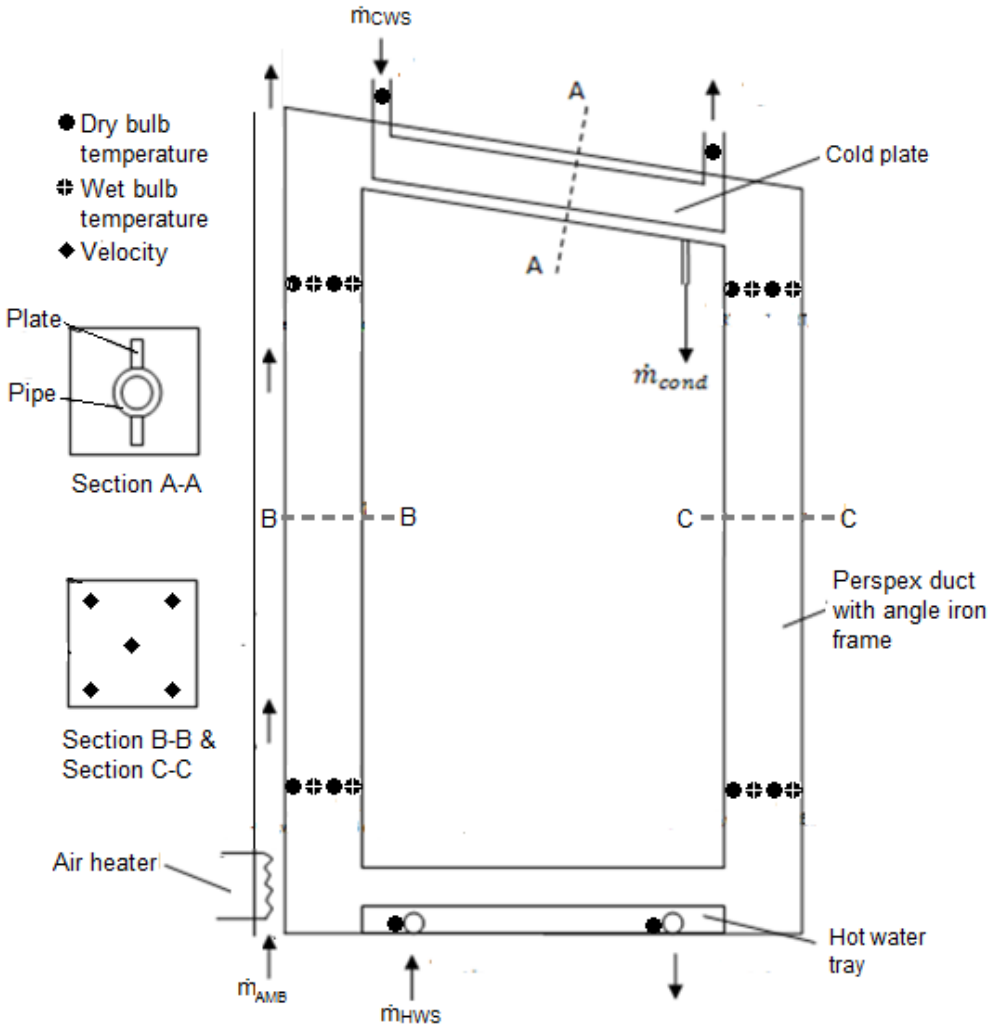

Figure 8 Model A schematic

The larger TDNCWP experimental loop 'model B' is shown in Figure 9. This model is a working TDNCWP system of large dimensions developed over the course of this project. The design is therefore based on the same configuration as small model A, with heated wall, hot water tray and cold plate in the same sections. It has a similar duct construction from angled iron and acrylic plastic sheeting and is of 400 mm x 400 mm duct cross section. The acrylic plastic is again utilized to view the flow conditions within the loop. However, the overall height, width, water tray area and cold plate area are increased in model B. The entire model B loop is broken into modules which are bolted together. This aids the manufacturing, transport and assembly of the loop. The water tray heat exchanger and the cold plate are connected to the same piping networks as used for model A. The cold plate is housed in the condensation section at the top. The cold plate is comprised of a central aluminium pipe with flat aluminium plates welded to it. Aluminium is used because of its high thermal conductivity and light weight. Like model A, cold water is circulated through it has using a cold water supply system. This is done to maintain a cool temperature relative to the internal humid air. Condensation is collected at the lower end of the condensate, where it runs though a gap in the ducting into a gutter system. The water tray is housed in the evaporation section. It has a copper pipe heat exchanger connected to a hot water supply system by piping in order to maintain the hot water temperature in the tray. It also has a 50mm foam insulation layer below it as shown in order to reduce losses to the ground. This tray is manually filled with fresh water, with the water surface exposed to the humid air within the TDNCWP loop. The heated wall for model B is comprised of four heating modules with internal aluminium sheets. These run from the bottom corner to the top corner of the heating section shown in Figure 9. Four independent 3 kW elements are attached to the outside of these panels, bolted against the aluminium panels with good contact by mild steel

backing plates with 50 mm glass fibre insulation. A schematic indicating the measurement points for model B is shown in Figure 10. The cross sectional velocity of the internal air is monitored at the top and bottom of the heating and cooling sections at nine grid points across a planar grid. This is done to find the velocity profile and the average velocity. Forty type-t thermocouples are placed around the loop. The internal dry and wet bulb temperatures are monitored in every section, across the width of the duct such that the average temperature and vapour concentration can be determined. The power input of the four aluminium heating walls is adjusted by rheostats and the temperature of each internal heating module wall is also monitored. In addition to the supply and return temperatures, the water of the hot water tray as well as the temperature of the cold plate surface are monitored. Two additional thermocouples are utilized to record the ambient dry and wet bulb temperatures at loop mid-height.

Figure 9 Picture of model B

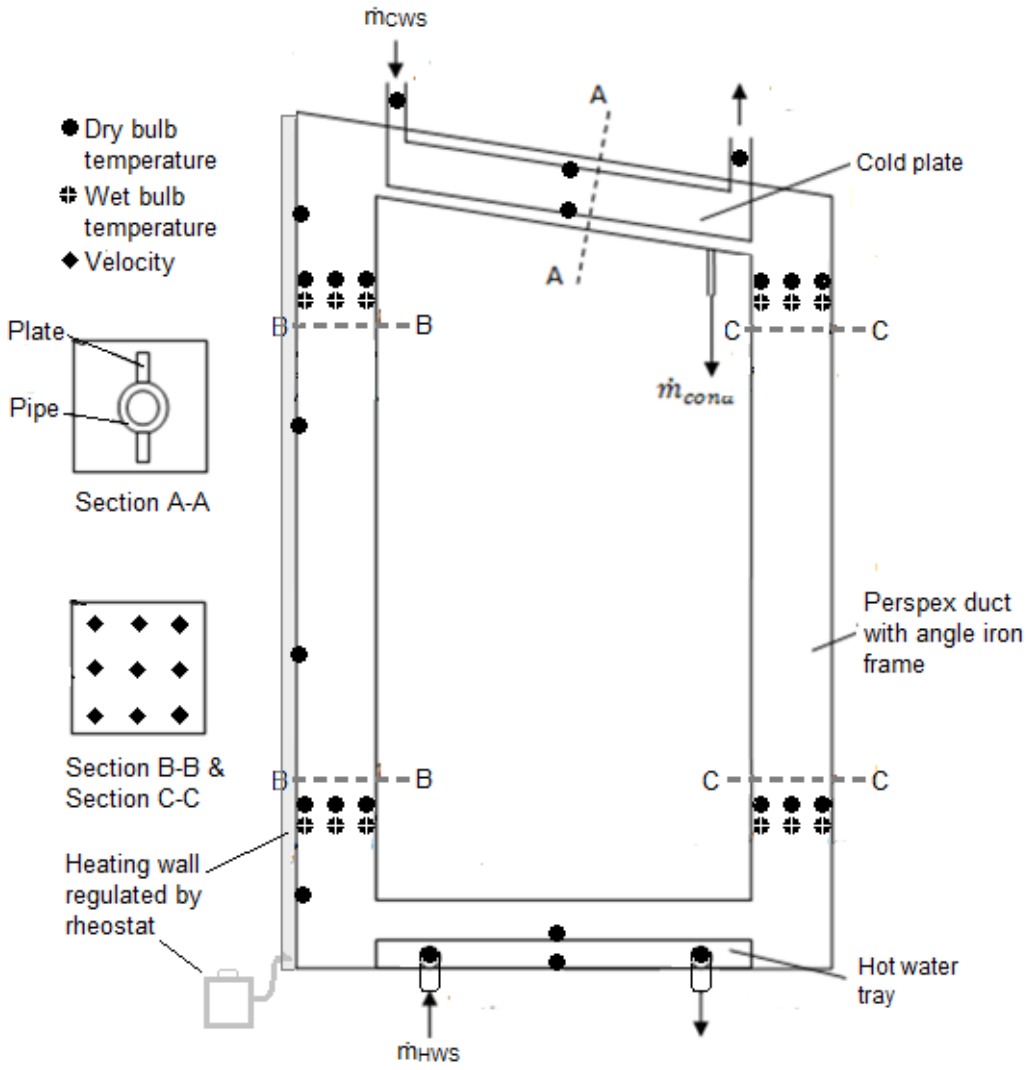

Figure 10 Model B model schematic

Type-T thermocouples are utilized in the measurement of temperature in both experimental models. Calibration was performed on all thermocouples in both models to reduce the measurement errors. In addition to the temperatures the velocity of the fluid is measured by use of a hot wire anemometer. By using the measured velocity and the density the mass flow rate can be found. The measurements are taken at a number of points in a grid at specific cross sections in the model shown in Figure 8 and Figure 10. The anemometer is configured to measure the flow in a certain direction only, so possible recirculation must be monitored. The bulk flow direction is checked by injecting non-reacting smoke into the flow within the loop. The flow rate of water in the cold water plate system and hot water tray systems are additionally measured. Six principle experiments were conducted on both models by applying set temperatures to the hot water tray supply temperature T_{HWS} and cold plate supply temperature T_{CWS}. The mass flow rate in the hot water and cold water supply systems is kept high, such that the supply and return temperatures to and from the TDNCWP are approximately equal. The experiments conducted are shown in Table 3. Utilizing the set temperatures in Table 3, the same six experiments were conducted on the experimental models of both model A and model B. They were conducted for ambient temperatures and ambient relative humidities in the range of 18 to 20 °C and 65 to 75% respectively. The heated wall was maintained at an average of 65 °C, which was verified by thermocouple measurements. During the experiments, the internal dry bulb and wet bulb temperature measurements were recorded at 1 minute intervals. In addition, the velocity and condensate measurements were regularly taken. Steady state conditions were then observed by comparing the measurements over time. However, verification of steady state conditions was found by calculating the energy balance of the system. The data collected from the experiments is processed such that the average loop temperature difference and velocity as well as the velocity profiles and the overall condensate rate can be

presented. This information is then utilized to calculate all other parameters required, such as the mass flow rate or energy transfer.

Table 3 Experiment set temperatures

Experiment	Set temperatures	
	T_{HWS} °C	T_{CWS} °C
1	50	18
2	60	18
3	70	18
4	50	10
5	60	10
6	70	10

The pumping performance of the TDNCWP can be evaluated by its condensate output, which is amount of water it supplies. This allows for comparison of different TDNCWP systems. However, condensate output this cannot fully evaluate the performance of the system. As the TDNCWP does not have an electrical energy source or the design requirements of a traditional water pump an experimental performance factor is therefore proposed. This performance factor, called the energy utilization factor (EUF), is the ratio of the mass of condensate produced to the heat energy required. At steady state, this heat added to the system will be equivalent to the heat energy extracted. The following is therefore proposed:

$$EUF = \frac{useful\ mass\ output}{energy\ \ added} = \frac{\dot{m}_{cond}}{(\dot{Q}_{\ evap\ section,NET} + \dot{Q}_{heat\ section,NET})} \quad (39)$$

EUF then represents the net heating and cooling energy in kJ required to produce a kg of condensate at steady conditions. This performance factor is dependent on the hot water tray and cold plate supply temperatures, as well as the geometry of the TDNCWP loop.

5 RESULTS

Experiments were conducted on the two experimental models as discussed and corresponding numerical results were additionally found. The loop temperature difference induces the density driven buoyancy force necessary for natural circulation flow and is more important than the absolute loop temperatures in understanding the overall system.

Loop temperature difference: The loop temperature difference is seen to be effected by the hot water tray and cold plate supply temperatures in both models. An average temperature difference of approximately 13 °C is observed for model A. The lower cold plate supply temperature resulted in a higher variance in temperature difference in the model with each of the hot water tray cases. In contrast, an overall temperature difference of approximately 4 °C is observed for model B, with the effect of the cold plate additionally reduced. The temperature difference was over predicted by the numerical model for the smaller loop, and under predicted in the larger loop. This may have implications on the numerically predicted condensate production rate and flow velocity. The temperature difference between the left hand heating and right hand cooling columns, discussed later in section 6.1, induces the natural circulation flow and velocity.

Loop flow rate: The flow rate is also affected by the wall friction. This wall friction is as a result of the flow velocity profile and its interaction with each wall, and may affect the overall condensate rate output. The velocity in the TDNCWP models was therefore determined during the experiments. This was done by anemometer measurement at cross section locations. At each cross section, it was measured across a planar grid. An experimental velocity contour plot was then generated for each cross section at steady conditions to indicate the flow distribution at those locations. The velocity contour plots for model A at a cold plate supply temperature of 18 °C is shown in Figure 11. It can be seen that the left hand heating section has a gradient in

the velocity profile across the cross section, with a higher velocity near the heated wall. This resembles those found in literature for a similar cases and implies a higher flow rate in that area of the duct. By smoke injections, the flow was observed to move from the hot water tray to the heated wall side of the duct as it exits the linking elbow and accelerate due to the heating. The flow also displays a fairly symmetrical profile with duct depth, across the midplane of the TDNCWP loop. Figure 11 further indicates that for lower hot water tray supply temperatures the velocity in the cooling section exceed that in the heating section. This unexpected response may be owing to the cooling effect at the cold plate being more significant when the TDNCWP heating inputs are lower. However, at increased hot water tray supply temperatures the velocity in the heating section exceeds that in the cooling section. The gradient in velocity across a cross section is more pronounced at increased hot water tray and lower cold plate supply temperatures. Similar trends are seen in the velocity around the loop for the large model B. However, the gradient in velocity is much greater. The velocity contour plots for model B at a cold plate supply temperature of 10 °C and a hot water tray supply temperature of 70 °C is seen in Figure 12. It is noted that a fully developed profile does not develop for both model A and model B for all set temperature cases at all loop points, with the exception of the bottom of the cooling section of model B under certain conditions. Otherwise, a non-symmetrical velocity profile that changes with flow direction is seen in both models. The flow is approximately symmetrical with duct depth, however, a gradient in the profile is observed in the heating section of each model. These effects are more noticeable at increased hot water tray and decreased cold plate supply temperatures and may lead a one-dimensional flow assumption being incorrect, particularly for a larger cross sectional width. An average experimental velocity of approximately 0.45 m/s is seen in all cases in the small model A loop and around 0.3 m/s in the model B loop. There is however some variation with the hot water tray and cold plate supply temperatures. Although the numerical model predicts the temperature difference to a reasonable accuracy for both model A and model B, the velocity for model B is still over predicted. This infers that the calculated frictional force is too low in the model B numerical model, which is due to the asymmetrical velocity profile observed during experiments not being accounted for.

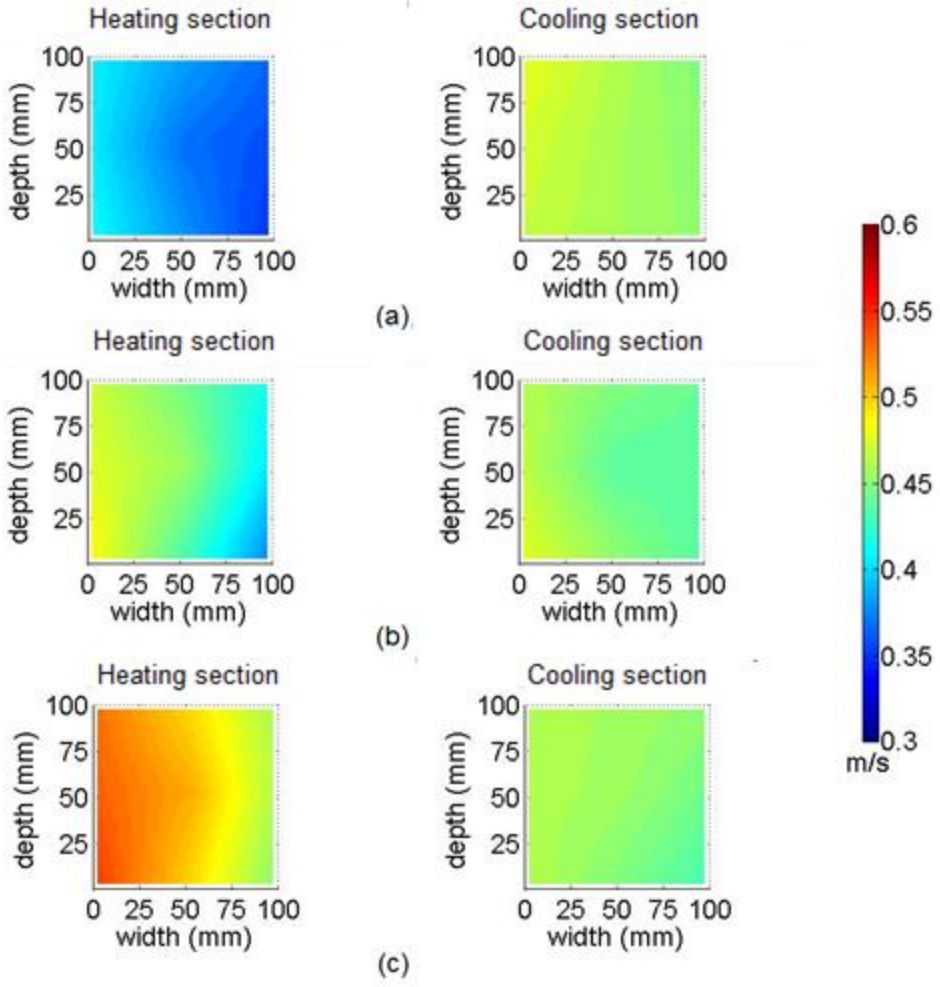

Figure 11 Cross sectional velocity profile at loop mid-section height for T_{cws} = 18 °C and (a) T_{hws} = 50 °C, (b) T_{hws} = 60 °C and (c) T_{hws} = 70 °C

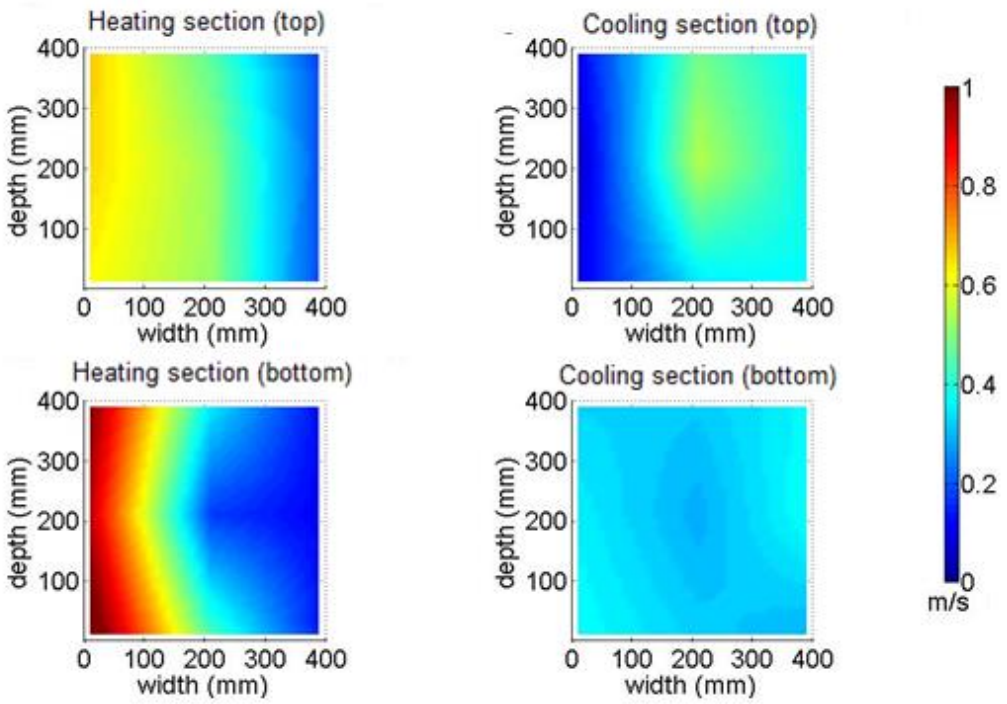

Figure 12 Cross sectional velocity profile normal to loop axis at top and bottom of cooling and heating sections for T_{cws} = 10 °C and T_{hws} = 70 °C

Loop flow rate: Condensate rate development is influenced by the internal air flow properties and the set supply temperatures of the hot water tray and cold plate and is therefore determined during the six experiments by measuring the condensate output at time intervals. The condensate rate increases with increasing hot water tray supply temperature as expected. This effect encompasses the overall air velocity and temperature increase explored previously, but also is as a result of the increased evaporation rate possible at higher hot water tray supply temperatures. Similarly, the condensate rate increases with decreasing cold plate temperature. It is noted though that the absolute condensate rate has a higher dependence on the hot water tray supply temperature than the cold plate supply temperature. Utilizing the experimental and numerically attained results, the steady water delivery rate for each of the experimental set temperatures is presented in L/day in Figure 13 for model A and Figure 14 for model B. The water delivery rate is based on 10 hours operation per day. It is interesting to note the approximately linear increase with hot water tray supply temperature in both the models. The magnitude of the numerical model over-prediction for both the experimental models is also better observed, with model A's numerical results up to 0.5 times higher and model B's up to 2.5 times higher. The numerical model tends to over predict the condensate rate for all hot water tray and cold plate supply temperatures, with the effect more noticeable when the former is increased. This over-prediction is worse for the larger width of model B, as a result of the over predicted velocity. However, the numerical model predicts the condensate rate of the experimental model A with reasonable accuracy, and predicts the same response as the experimental data to the increasing hot water tray and decreasing cold plate supply temperatures for both model A and model B. A higher dependence on the hot water tray supply temperature is noted, which is a consequence of both the increased evaporation rate and increased velocity at higher hot water tray supply temperatures.

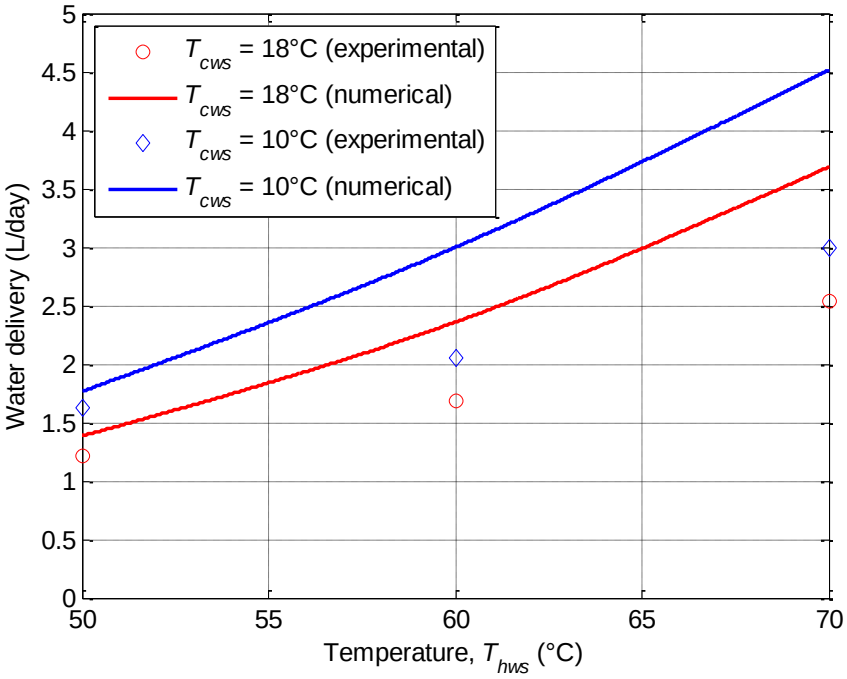

Figure 13 Model A steady water delivery per 10 hour day

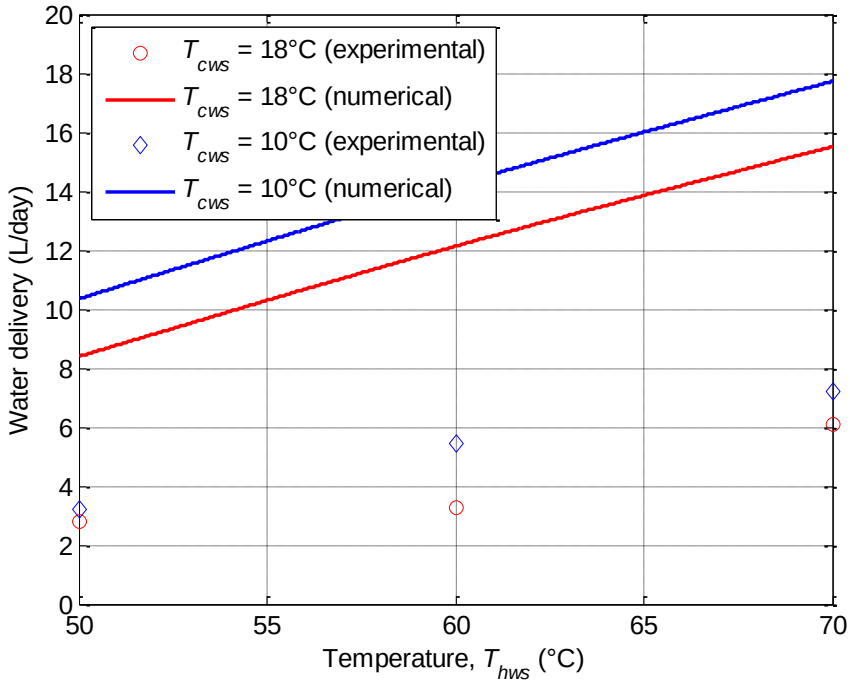

Figure 14 Model B steady water delivery per 10 hour day

System performance: The TDNCWP performance is determined from experimental and numerical results. This is done not only to evaluate the TDNCWP system, but to compare the experimental models discussed. The EUF is calculated based on the condensate collected, and the energy balance results shown in appendix B2, both of which are based on data collected during the experiments. The result is presented for model A in Figure 15 and for model B in Figure 15 for the various set temperatures. The figure indicates that less energy is required to be added and removed for the lower cold plate and, more significantly, at higher hot water tray supply

temperatures. The two cold plate temperatures do, however, display a similar linear trend. The EUF for model B is shown for the varied set temperatures. The linear increase indicated for model A is not seen here, with both temperatures having a curved profile. The trends indicate that more energy is required to produce a kg of condensate for the larger model. This is due to the higher loop volume and asymmetrical flow velocity discussed in section 6.2. For the cold plate supply temperature of 18 °C the EUF initially decreases then increases again with increasing hot water tray supply temperature. For the cold plate supply temperature of 10 °C, the trend is increasing always with the gradient diminishing. The strange behaviour in the EUF for model B is as a result of the energy exchange at the heating section changing at a different rate to the energy exchange at the evaporation sections. Nevertheless, the decreased cold plate supply temperature generally provides a higher condensate supply per kJ of energy.

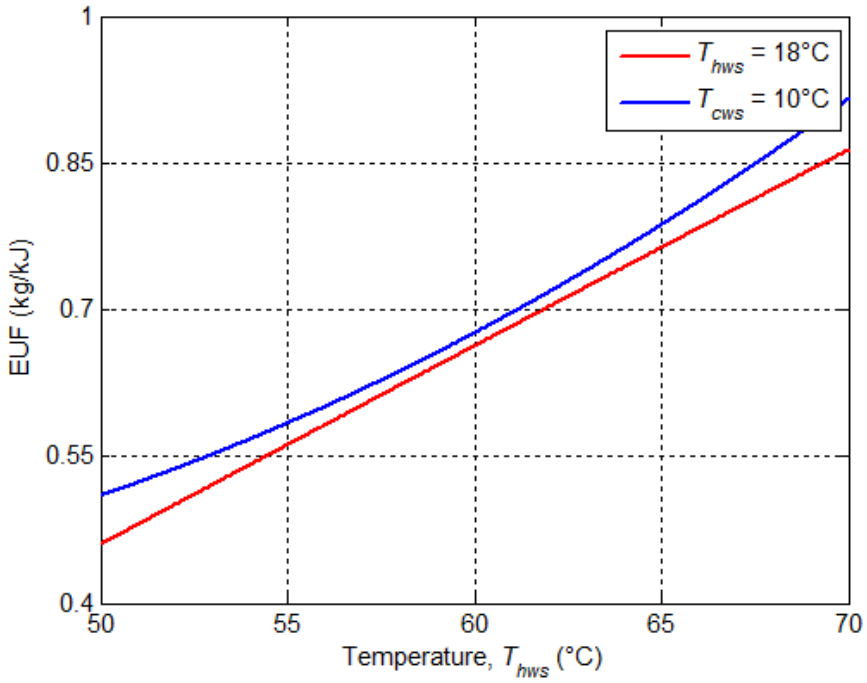

Figure 15 Model A energy utilization factor

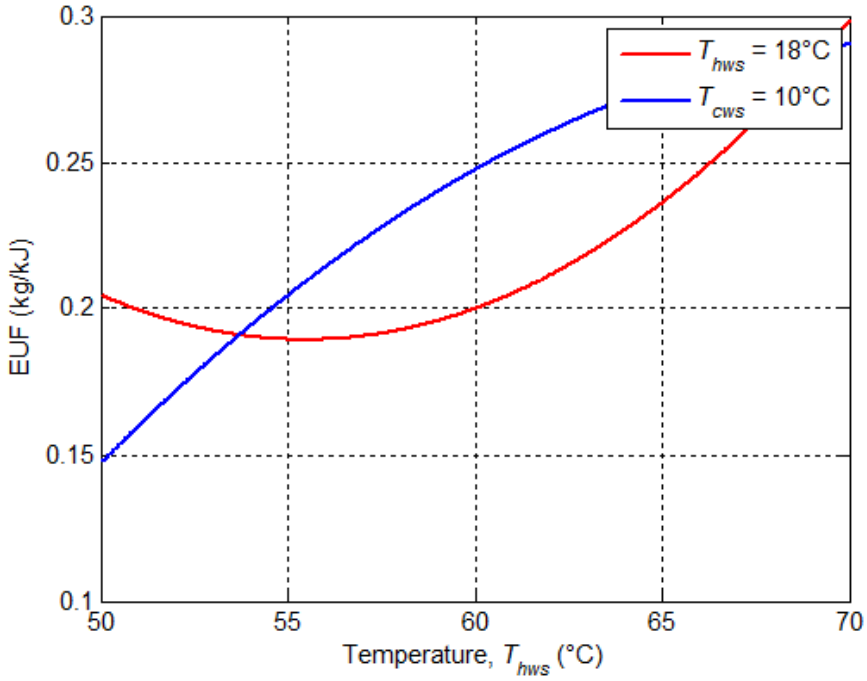

Figure 16 Model B energy utilization factor

Further consideration into loops of varied size provides insight into the feasibility of the TDNCWP system. The numerically generated steady condensate rate versus the duct width for fixed overall loop dimensions and set temperatures is shown in Figure 17. The condensate rate is seen to increase with increasing duct width to some asymptotic value, where the maximum amount of water is extracted from the humid air. At a lower duct width the condensate rate decreases, due to the loop mass flow rate being lower with decreased cross sectional area for a similar velocity and the mass transfer areas too small for the loop volume. However, due to the numerical model limitations discussed in section 6.3, the prediction at these lower widths is likely more accurate than at higher widths. The condensate rate is also seen to increase with increasing TDNCWP loop size. This is due to the cold plate, hot water tray and heated wall dimensions increasing too, and the additional duct friction induced being lower than the additional natural circulation buoyancy force.

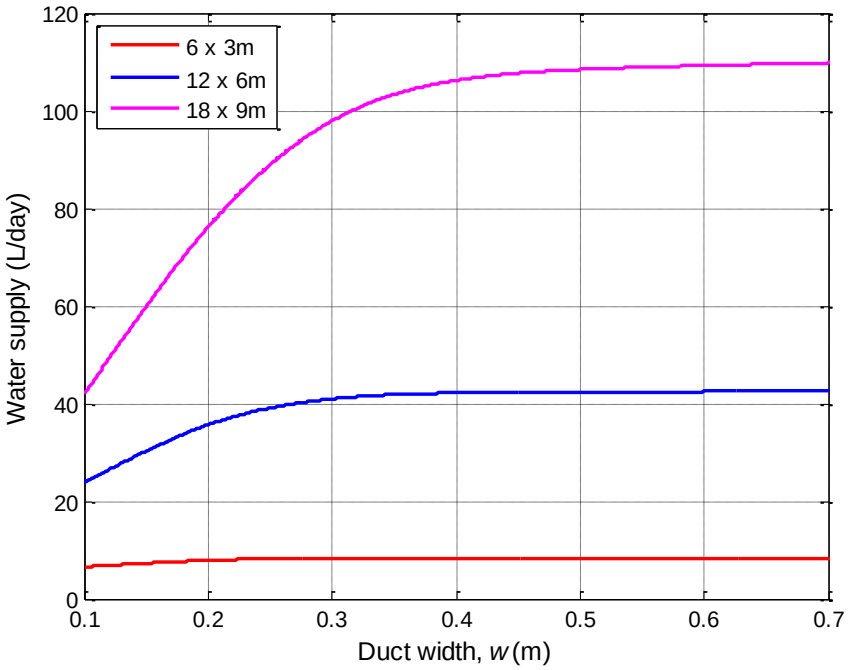

Figure 17 Condensate rate for varied duct and TDNCWP loop size at T_{cws} = 18 °C and T_{hws} = 50 °C

6 CONCLUSIONS

The TDNCWP configuration that was designed and built for experimental purposed was comprised of four square duct sections with four major components: a hot water tray, a cold plate, a heated section and a cooled section. A one-dimensional numerical model was additionally written, and validated against the experimental results. The following conclusions can be drawn:

1. A large link between the velocity rate and profile and the overall pumping rate is observed. An increased velocity will improve the condensate output significantly. This increased velocity insures water is evaporated, moved to roof level and then condensed at a higher rate. The velocity can be increased by increasing the buoyancy force or decreasing the internal flow friction, particularly the swirling flow at the elbows which was observed during smoke tests. An asymmetrical velocity profile is found for both models with a higher gradient in this profile was more noticeable at greater loop dimensions as well as increased hot water tray and decreased cold plate supply temperatures. The effects of the asymmetrical velocity profile on the overall condensate rate can be mitigated by use of smaller width loops. The flow was however observed to have some symmetry across the TDNCWP midplane, and axisymmetrical flow at the end of the large model cooling section under certain conditions. The bulk flow direction in the TDNCWP configuration surmised is parallel to the walls and in the clockwise direction, although with some swirling and erratic flow particularly after the elbows and at the heated surfaces due to secondary buoyancy driven flows and the elbows.
2. The energy required for each unit of water supplied decreases with decreasing duct width. This infers that multiple independent narrow-width loops should be used parallel to deliver the required water rather than a larger width loop. It is assumed however that the same passive heating and cooling is available in both circumstances.
3. The water delivery rate was additionally found by experiment to depend more on an increased hot water tray supply temperature that a decreased cold plate supply temperature. Increasing the surface area of either mass transfer surface will also assist; however, efforts should be focused on the hot water tray surface. This could possibly be facilitated practically by splitting the water tray into a few smaller, independent water trays.

4. The one-dimensional model is inaccurate in its prediction of the condensate rate at higher cross sectional widths, and more accurate at lower cross-sectional widths. This effect is linked to a similar trend in the velocity prediction. It does, however, predict the trends well for varying set temperatures
5. Utilizing the TDNCWP independently in its current configuration to supply the required water for PDEC systems may not be feasible for larger buildings due to the number of systems required. This deduction is based on the limited data for currently available for PDEC system water requirements, where excess water is utilized. In these larger buildings, the TDNCWP system could perhaps be used to supplement the existing pumping system and reduce electrical usage and pumping costs. It would additionally continue to operate should electricity supply fail. However, the TDNCWP in its current design could be independently applied to smaller building PDEC systems such as residential houses, or systems where electricity is not available and optimal PDEC performance is not critical.

7 RECOMMENDATIONS

The following recommendations can be made:

1. Conduct experimental tests with the existing model A and/or model B loop(s) connected to a passive means of hot water tray heating and cold plate cooling, with exposure to varied heated wall and ambient temperatures. These will give a further indication of the TDNCWP response and feasibility in the intended usage scenarios.
2. Modify the experimental set-up to include guide vanes and different hot water tray, cold plate and elbow configurations. This design should aim to increase the flow rate by ordering the flow after corners. The condensate rate can further be increased by directing the airflow towards mass transfer surfaces.
3. Expand the current theoretical model to a two-dimensional model to incorporate the effects of varying temperature, velocity and concentration across the duct width. A two-dimensional assumption may model the outputs as higher widths to a greater accuracy.
4. Perform a CFD numerical study to visualize and optimize the flow within the loop.
5. Perform a feasibility study where a TDNCWP is designed and built to complement a specific PDEC systems requirements.

Nomenclature

A	Area
B	Gravitational force term
C	Constant
C_f	Friction coefficient
c_p	Specific heat at constant pressure
D_h	Hydraulic diameter
D_{v-a}	Diffusion coefficient for water vapour into air
E	Total energy
EUF	Energy utilization factor
F	Friction term
G	Volumetric flow rate
g	Gravity
h	Enthalpy
h_{fg}	Latent heat of vaporization
h_g	Vapour saturation enthalpy
h_{ht}	Heat transfer coefficient
h_{mt}	Mass transfer coefficient
i	Control volume number
k	Conductivity
L	Length

m	Mass
$\dot{m}$	Mass flow rate
M	Mass term
M_M	Molar mass
$M1$	Momentum change term 1
$M2$	Momentum change term 2
N	Total number of control volumes
P	Pressure
p	Perimeter
$\dot{Q}$	Heat transfer rate
R	Thermal resistance
R_a	Gas constant of air
R_v	Gas constant of water vapour
T	Temperature
T1	Temperature change term 1
T2	Temperature change term 2
t	Time
u	Internal energy
V	Volume
v	Velocity
$\dot{W}$	Work rate
w	Width
x	Duct length
x_v	Mass fraction
z	Height

Δ	Difference
β	Coefficient of volumetric expansion
ϵ	Relative surface roughness
θ	Angle relative to the horizontal
μ	Dynamic viscosity
ρ	Density
Σ	Summation
τ	Shear stress
ϕ	Relative humidity
ω	Specific humidity

SUPERSCRIPT:

$\bar{v}$	Mean
$\vec{v}$	In all Cartesian directions
t	At time t
Top	At the top
Bottom	At the bottom

SUBSCRIPT:

a	Air
av	Average at cross section
cws	Cold water supply
c	Cross section

ch	Characteristic
CS	Control surface
CV	Control volume
cd	Conductivity
$cond$	Condensation
$conv$	Convective
$cool$	Cooling section
exp	Experimental
$fluid$	Of the flowing fluid
hw	Heated wall
hws	Hot water supply
hd	Hydrodynamic
ht	Heat transfer
$heat$	Heating section
i	At control volume i
in	Into control volume
$inner$	Inside surface
lam	In the laminar flow regime
$minor$	Minor losses
mt	Mass transfer
NET	Overall into control volume
$natural$	Due to local natural forces
nm	Numerical
out	Out of control volume
$other$	Other than those specified
$outer$	Outer surface
R	Resultant
sat	At saturation condition
S	Maximum amount of surfaces
s	At or applied to surface
sys	Of the entire system
tc	Thermocouple
$turb$	In the turbulent flow regime
v	Vapour
$wall$	Of the wall

Acknowledgements

I would like to thank the NRF for the funding of this project.

Reference

1. Green building council of South Africa, s.a., *About green building* [Online]. Available: https://www.gbcsa.org.za/about/about-green-building/ [14 September 2014].
2. Milford, R. 2009. *Greenhouse gas emission baselines and reduction potentials from buildings in South Africa*. Paris: United Nations Environment Programme.
3. Eskom demand side management. 2013. *DSM 0002: Air-conditioning facts.* [Online]. Available: http://www.eskom.co.za/content/ DSM_0002AirConFactsRev5.pdf. [25 July 2013].
4. Mathews, E.H., Botha, C.P, Arndt, D.C. & Malan, A. 2001. HVAC Control strategies to enhance comfort and minimize energy usage. Energy and Buildings 33.1: 853-863.

5. Fuller, S. 2010. *Life-cycle cost analysis (LCCA).* National Institute of Standards and Technology. [Online]. Available: http://www.wbdg.org/resources/lcca.php. [25 May 2014].
6. Austin, S. B. 1997. HVAC System trend Analysis. *ASHRAE Journal* 39.2: 44-50.
7. Bowman, NT., Lomas, K. J., Cook, M. J., Eppel, H., Robinson, D., Ford, B., Diaz, C., Wilton, O., Cucinella, M., Badano, E., Bombardi, F., Francis, E., Galatà, A., Lanarde, P., Belarbi, R., Rodríguez, E. & Álvarez, S. 1998. *The Application of Passive Downdraught Evaporative Cooling (PDEC) to Non-domestic Buildings*. [Online]. Available: http://www.phdc.eu/uploads/media/PDEC_3_Publishable_ final_report.pdf [22 May 2014].
8. Kang, D. & Strand, R.K. 2009. 'Simulation of Passive Down-Draught Evaporative Cooling (PDEC) Systems in Energyplus'. Paper presented at *Eleventh International IBPSA Conference,* Glasgow, Scotland, 27-30 July.
9. Guedes, M.C. & de Melo, A.C.M. 2006. *Passive Downdraught Evaporative Cooling Applied on Existing Fabric: Using Traditional Chimney as Case Study in Portugal* . [Online]. Available: http://pleaarch.org/ARCHIVE/2006/Vol1/ PLEA2006_PAPER129.pdf. [22 May 2014].
10. Robinson, D., Lomas, K.J., Cook, M.J. & Eppel, H. 2004. Passive down-draught evaporative cooling: thermal modelling of an office building. *Indoor and Built Environment*. 13.3: 205-221.
11. Kang, D. 2011. 'Advances in the application of passive down-draft evaporative cooling technology in the cooling of buildings'. Paper submitted for Doctor of Philosophy. University of Illinois, Urbana-Champaign.
12. Barletta, A E., di Schio, R. & Zanchini, E. 2003. Combined forced and free flow in a vertical rectangular duct with prescribed wall heat flux. *International journal of heat and fluid flow* 24.1: 874-887.
13. Smith, R. 2013. *Turning vanes required.* [Online]. Available: http://www.symscape.com/blog/turning-vanes-required [July 17 2014].
14. Chou, F.C. (1989). Effect of nonuniform heating on laminar mixed convection in the entrance region of horizontal ducts. *Computers & Fluids* 17.3: 487-496.
15. Lin, J.N., Tzeng, P.Y., Chou, F.C. & Yan, W.M. 1992. Convective instability of heat and mass transfer for laminar forced convection in the thermal entrance region of horizontal rectangular channels. *International journal of heat and fluid flow* . 13.3: 250-258.
16. Sartori, E. 2000. A critical review on equations employed for the calculation of the evaporation rate from free water surfaces. *Solar Energy*. 68.1: 77-89.
17. Asdrubali, F. 2009. A scale model to evaluate water evaporation from indoor swimming pools. *Energy and Buildings* 41.1: 311-319.
18. Smith, C.C., Jones, R.W. & Lof, G . 1993. Energy Requirements and Potential Savings for Heated Indoor Swimming Pools. *ASHRAE Transactions*. 9.2: 864-874.
19. Smith, C.C. & Lof, G . 1999. Rates of evaporation from swimming pools in active use. *ASHRAE Transactions*. 104.1A: 514-523.
20. Shah, M.M. 2002. Rate of Evaporation from Undisturbed Water Pools: Evaluation of Available Correlations. *International Journal of HVAC&R Research*. 8.1: 125-131.
21. Shah, M.M. 2003. Prediction of evaporation from occupied indoor swimming pools. *Energy and buildings* . 35.7: 707-713.
22. Iskra, C.R. & Simonson, C.J. 2007. Convective mass transfer coefficient for a hydrodynamically developed airflow in a short rectangular duct. *International journal of heat and mass transfer*. 50.1: 2376-2393
23. Cengel,Y.A. & Ghajar, A.J. 2011. *Heat and Mass transfer: Fundamentals and applications.* 4ed. New York: McGraw Hill.
24. Tsilingiris, P.T. 2009. Thermophysical and transport properties of humid air at temperature range between 0 and 100degC. *Energy conversion and management*. 49.1: 1098-1110.